I&EC research
Industrial & Engineering Chemistry Research
pubs.acs.org/IECR
Article

Olive Waste Valorization Through TGA-MS Gasification: A Diatomaceous Earth Effect

María Puig-Gamero, Luz Sanchez-Silva,* and Paula Sánchez

Cite This: *Ind. Eng. Chem. Res.* 2021, 60, 7505−7515

ABSTRACT: The effect of diatomaceous earth on gasification of olive pomace and olive stone was studied by thermogravimetric analysis with mass spectrometry (TGA-MS). Additionally, gas emissions, the H_2/CO ratio, and gasification reactivity were evaluated. First, a preliminary study of the effect of particle size on olive waste gasification was performed to select the most appropriate from a technical and industrial point of view. With olive pomace, the larger the particle size, the lower H_2/CO and reactivity. However, with olive stone, optimum results were observed with the largest particles. Subsequently, olive waste was mixed with different percentages (10, 25, and 50 wt %) of diatomaceous earth. When olive pomace contained diatomaceous earth, even though there was no substantial improvement in reactivity, syngas quality in terms of H_2/CO was significantly enhanced and increased by up to four times. However, the diatomaceous earth effect on olive stone gasification was more remarkable, enhancing both reactivity and the H_2/CO ratio. Different behaviors in the biomasses were due to the different impacts of the alkali and alkaline earth metals on the diatomaceous earth. Whereas both of these made positive contributions to the olive stone, only the latter had a significant influence on olive pomace.

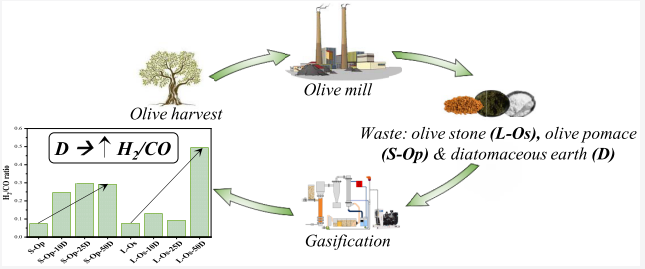

1. INTRODUCTION

According to the European Commission, Spain is the world's leading olive oil producer and exporter, accounting for about half of total global production.[1] Although this industry is characterized by producing significant economic benefits for the country, it is also known for the high amount of waste, mainly olive pomace and olive stone, it generates. These can be up to four times higher than the end product, which causes severe environmental damage due to the high quantity of waste and difficulty in treating it.[2,3] Although olive stone is used as a low-cost solid biofuel, mainly for conventional combustion, as yet there is no definitive market or use for olive pomace. Thus, olive oil producers need to find a technologically feasible, environmentally friendly, economically viable, and socially acceptable solution to this problem.[4,5]

In this framework, olive waste gasification is an attractive option and an alternative to biomass combustion mainly for local uses since this enables the biomass to be used close to its source, and thus, to eliminate many costs associated with storage and transportation.[6−8] Moreover, after it has been cleaned adequately, the gas from biomass gasification can be burnt directly for subsequent use as a fuel in internal combustion engines or gas turbines.[9] Alternatively, producer gas can also be used in fuel cells and as a feedstock to produce biofuels and chemicals with an added value.[10]

In this regard, some recent studies have focused on gasification for valorizing olive waste. González-Vázquez et al.[11] compared gasification of unconventional types of biomass, including olive stone with the most traditionally used biomass, pine sawdust, in a bubbling fluidized bed. Olive stone showed comparable results to pine sawdust.[11] Castro et al.[12] analyzed the potential of olive pomace in air gasification and determined the optimal gasification parameters. Puig-Gamero et al.[13,14] studied catalytic and noncatalytic gasification of olive pomace, coke, and petcoke, and reported olive pomace had the highest reactivity and gas quality. Moreover, the reactivity of the blends and the H_2/CO ratio increased in line with the amount of olive pomace in the blend. In addition, these results improved when dolomite was used as a catalyst in gasification.[13,14] Almeida et al.[15] carried out olive pomace gasification in a fluidized bed reactor and concluded that higher bed temperatures favored gas production and made gasification more efficient. Cardoso et al.[16] presented a technoeconomic analysis of olive pomace gasification coupled with cogeneration for two sizes of the gasifier (100 and 1000

Received: February 16, 2021
Revised: April 29, 2021
Accepted: April 29, 2021
Published: May 9, 2021

https://doi.org/10.1021/acs.iecr.1c00688
Ind. Eng. Chem. Res. 2021, 60, 7505−7515

Table 1. Ultimate Analysis, Proximate Analysis, and Mineral Content of the Olive Pomace, Olive Stone, and Diatomaceous Earth Samples[a]

	proximate analysis (wt %)*daf				ultimate analysis (wt %)*daf				
	moisture	ash	volatile matter	fixed carbon*diff	C	H	N	O*diff	S
olive pomace (Op)	2.12	7.77	80.73	9.38	52.49	6.66	1.51	31.31	0.26
olive stone (Os)	7.91	1.95	69.25	20.89	49.88	6.12	nd	44.00	nd
	mineral content (g/L)								
	calcium (Ca)	potassium (K)	magnesium (Mg)	sodium (Na)	silicon (Si)	titanium (Ti)			
olive pomace (Op)	2.99	23.0	0.52	nd	100	0.03			
olive stone (Os)	nd	1.87	nd	nd	nd	nd			
diatomaceous earth(D)	12.2	1.45	5.20	0.05	801	1.10			

[a]*daf: dry and ash free basis; O^diff: % of oxygen calculated from differences in C, H, N, and S; fixed carbon*diff: % of fixed carbon was calculated from differences in moisture, ash, and volatile matter; and nd: nondetectable.

kW). Their results showed that the former was not economically viable, whereas the latter was.[16]

Moreover, diatomaceous earth is another little-known olive oil waste. It is widely used for separating crude oils from vegetation water, impurities, and any fatty substances to obtain extra virgin olive oil due to its low cost, retention capacity, and its half-life. However, once it reaches saturation, it should be valorized in an economical and environmentally friendly way. In this respect, diatomaceous earth can be valorized during gasification of olive pomace and olive stone since it could enhance the process due to its composition, which is mainly SiO_2, CaO, MgO, Na_2O, and K_2O. Moreover, it is common knowledge that these alkali metals can improve gasification performance.[17]

Nonetheless, despite all of the research carried out to date, there have been no studies on how diatomaceous earth affects gasification of olive pomace and olive stone. Thus, the novelty of this study lies in the use of diatomaceous earth in the gasification of olive pomace and olive stone to study how this process could be improved and to make a comprehensive evaluation of waste. In addition, not only might this study help to enhance this process and valorize residues from it but also to reduce the current linear economy based on "make, take, and dispose" while promoting the circular economy and preserving the environment. First, the effect of particle size was studied in olive pomace and olive stone to select the most appropriate one from a technical and industrial point of view. Subsequently, olive pomace and olive stone were mixed with different amounts of diatomaceous earth (10, 25, and 50 wt %) to evaluate their effect on gasification. Finally, a comparison was made in terms of reactivity, outlet-gas emissions, and the H_2/CO ratio of the effluent by means of a thermogravimetric analysis with mass spectrometry (TGA-MS) analysis.

2. MATERIALS AND METHODS

2.1. Materials. Olive pomace (Op) and olive stone (Os), provided by "Aceites Garcia de la Cruz" olive oil mill, Madridejos (Toledo, Spain), were the raw materials used in this research. These samples were oven-dried for 5 h, milled, and sieved within the range of 0.5−2 and 0.85−4 mm for olive pomace and olive stones, respectively. Additionally, used diatomaceous earth (D) was also obtained from Aceites Garcia de la Cruz olive oil.

The ultimate and proximate analyses were performed according to UNE standards 15104:2011, UNE−EN ISO18123, UNE 32-004-84, and UNE 32002-95, while metal contents in the samples were determined by inductively coupled plasma (ICP) spectrometry. The results of these analyses are listed in Table 1. Finally, Table 2 shows the characteristics of the raw materials in each experiment and the name used for identifying them.

Table 2. Characteristics and Identification of the Different Samples under Study

identification	sample	particle size (mm)	diatomaceous earth (wt %)
S-Op	olive pomace (Op)	0.5−0.85 (small)	
M-Op	olive pomace (Op)	0.85−1.4 (medium)	
L-Op	olive pomace (Op)	1.4−2 (large)	
S-Os	olive stone (Os)	0.85−1.4 (small)	
M-Os	olive stone (Os)	1.4−2 (Medium)	
L-Os	olive stone (Os)	2−4 (large)	
S-Op-10D	olive pomace (Op)	0.5−0.85 (small)	10
S-Op-25D	olive pomace (Op)	0.5−0.85 (small)	25
S-Op-50D	olive pomace (Op)	0.5−0.85 (small)	50
L-Os-10D	olive stone (Os)	2−4 (large)	10
L-Os-25D	olive stone (Os)	2−4 (large)	25
L-Os-50D	olive stone (Os)	2−4 (large)	50

2.2. Equipment and Procedures. *2.2.1. TGA-MS Analysis.* Steam gasification of the samples considered, herein, was carried out in a TGA apparatus (TGA−DSC 1, METTLER TOLEDO) coupled with a mass spectrometer (Thermostar-GSD 320/quadrupole mass analyzer, Pfeiffer Vacuum). Just like in the research reported in ref 18, the steam required was generated by passing the carrier gas (Ar) through the water contained in a system made up of four bubblers, which were connected in a series and immersed in a bath at a controlled temperature. The $Ar-H_2O$ mixture was assumed to be saturated, and a gas stream of 5 vol % water in Ar was obtained.

Steam gasification was performed in three different steps. First, the sample was preheated at 105 °C and then kept at this temperature for 10 min to remove its moisture. Then, pyrolysis was performed at temperatures ranging from 105 to 1000 °C at a heating rate of 40 °C/min and a constant flow of 200 NmL/min in an Ar atmosphere. Next, the samples were subjected to steam gasification under isothermal conditions (900 °C for 120 min). Finally, with the mass spectrometer, the compounds

https://doi.org/10.1021/acs.iecr.1c00688
Ind. Eng. Chem. Res. 2021, 60, 7505−7515

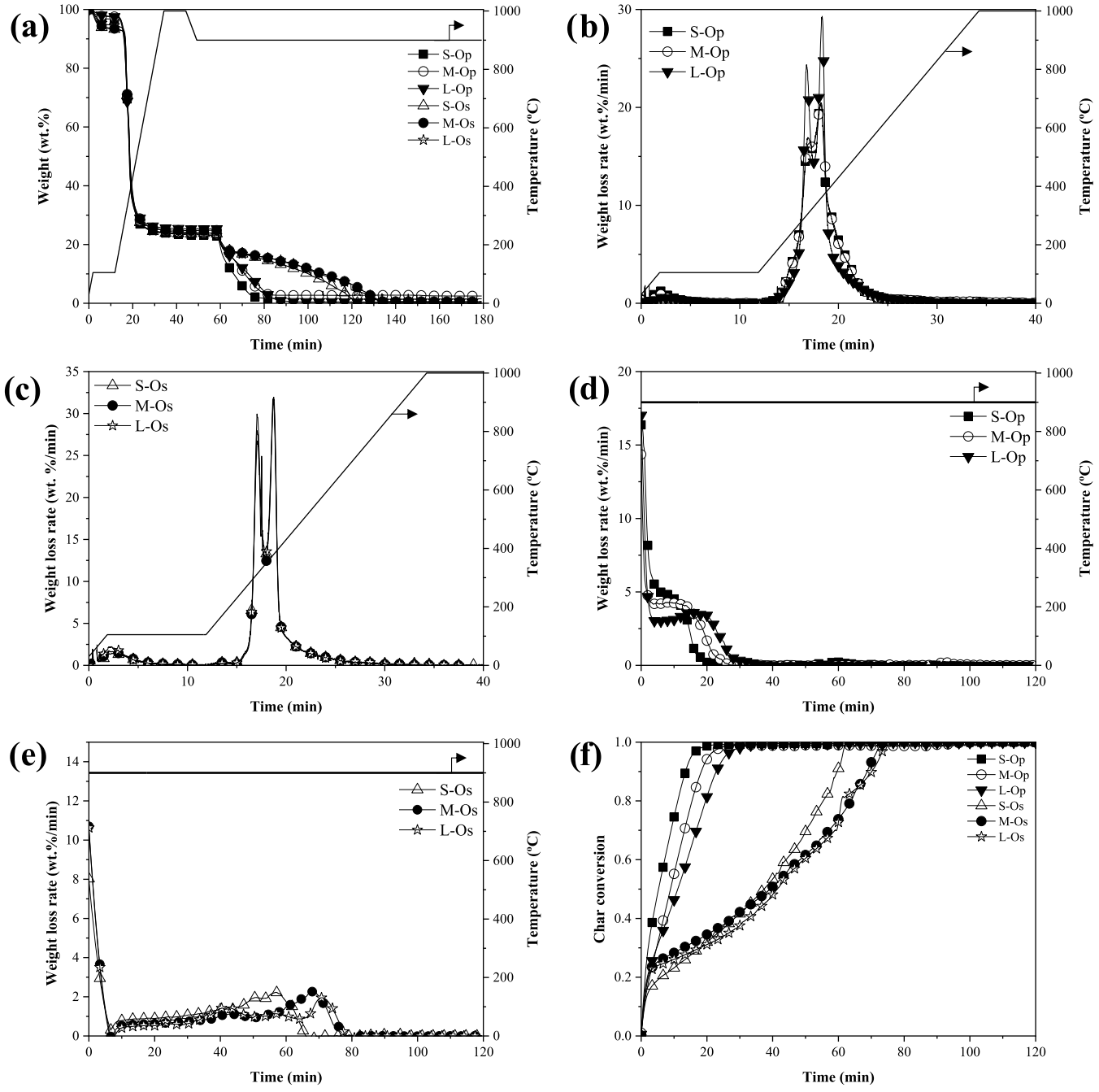

Figure 1. TGA/derivative TG (DTG) profiles for olive pomace and stone pomace gasification as a function of particle size: (a) TGA curves for gasification, (b) DTG curves for the pyrolysis of olive pomace, (c) DTG curves for the pyrolysis of olive pomace, (d) DTG curves for the gasification of olive pomace, (e) DTG curves for the gasification of olive stone, and (f) char conversion vs time plots for olive pomace and olive stone gasification.

released during thermal degradation of the sample could be identified and analyzed. The intensity peak areas between different samples were compared in a normalized procedure.[19] The initial sample weight was fixed at 20 mg, while the particle size range was varied (Table 2). In addition, each sample was analyzed at least three times, and the average value was recorded. The experimental error in temperature was ±2 °C, whereas the weight loss measurement was ±0.5 %.

2.2.2. Char Reactivity. Char reactivity was calculated with the following equation

$$R_i = -\frac{1}{w_i} \times \frac{dw_i}{dt} = \frac{1}{1 - x_i} \times \frac{dx_i}{dt} \quad (1)$$

where x_i and w_i are the conversion and weight of char at any time, respectively.

In this work, reactivity at 50% (R_{50}) and at 90% (R_{90}) of char conversion was considered for comparative purposes.[20−24]

3. RESULTS AND DISCUSSION

3.1. Preliminary Study. *3.1.1. Effect of Particle Size during Gasification of Olive Waste.* A preliminary study into the influence of particle size in terms of the H_2/CO ratio and

https://doi.org/10.1021/acs.iecr.1c00688
Ind. Eng. Chem. Res. 2021, 60, 7505−7515

gasification reactivity was carried out to select the most suitable particle size for both olive waste biomasses. Figure 1a shows the thermogravimetric analysis (TGA) for olive pomace and olive stone gasification as a function of particle size. This can be split into two main processes: pyrolysis and gasification. Weight loss at the pyrolysis stage (up to 60 min) was visibly higher than that observed during gasification. Moreover, slight differences between the raw materials and their different particle sizes were detected during pyrolysis. The main variations observed were associated with the drying stage and char formation. Conversely, results from gasification varied considerably. As expected, weight loss was faster in the olive pomace sample than in olive stone due to its higher volatile matter content (Table 1). Therefore, olive pomace was considered to be the more reactive raw material.

Figures 1b,c shows the DTG curves for the pyrolysis of olive pomace and olive stone as a function of particle size, respectively. As reported elsewhere,[25−28] the DTG curves revealed three common degradation stages. The first was associated with drying. The second represented the main pyrolysis stage and was attributed to devolatilization of the raw materials, both of which showed the highest weight loss at this stage. In addition, three shoulders could be distinguished at this point for both biomasses. This could be attributed to the individual decomposition of the main components of lignocellulosic in the following order: hemicellulose, cellulose, and lignin. The first stage was observed at temperatures around 300 °C, which was associated with hemicellulose decomposition. This shoulder was steeper for the olive stone, which can be linked to a higher hemicellulose content.[29] In the second stage, the maximum weight loss rate was obtained around 400 °C for both biomasses due to cellulose decomposition. At this stage, olive stone and olive pomace presented similar weight losses, which can reveal similar cellulose content.[29] Finally, this highest weight loss was followed by a tail, which was ascribed to lignin decomposition, which leads to char formation (third stage). As can be seen, the char yields were similar for both, thus, the lignin content was similar.

As for olive stone, the DTG profiles during pyrolysis for different particle sizes were similar and the curves overlapped so their effect could be considered insignificant. However, the DTG profile for olive pomace showed differences when particle size increased. It should be noted that olive pomace and olive stone are olive waste. Although they were separated, part of the smallest stone might have been swept away with the olive pomace. Therefore, the larger the amount of olive pomace, the more likely it was to contain particles of olive stone. Thus, it can be seen that while S-Op and M-Op had similar profiles, L-Op had a DTG curve, which was more similar to that for the olive stone. In addition, S-Op and M-Op showed a small shoulder at a high temperature, while this was not observed for L-Op. This may be associated with lipid decomposition from the olive oil contained in the olive pomace.[30,31]

Figure 1d,e shows the DTG curves for the gasification stage as a function of particle size. It can be seen that the gasification started as soon as the gasifying agent reached the surface of the char particle. Unlike in the previous stage, large differences were detected. For both biomasses, gasification was improved with smaller particle size. According to Tripathi et al., this fact could be related to an increase in the diffusion resistance in gasification when particle size increased.[32]

Furthermore, Table 3 lists the reactivity parameter at 50% (R_{50}) and 90% (R_{90}) of char conversion and the time required

Table 3. Gasification Reactivity of Olive Pomace and Olive Stone as a Function of Particle Size

sample	R_{50} (1/min)	t_{50} (min)	R_{90} (1/min)	t_{90} (min)
S-Op	0.11	5.6	0.39	13.5
M-Op	0.09	8.9	0.28	18.3
L-Op	0.06	11.1	0.25	22.8
S-Os	0.02	37.4	0.28	59.6
M-Os	0.02	39.2	0.25	68.7
L-Os	0.03	41.4	0.16	70.1

to achieve this conversion (t_{50} and t_{90}) in all samples. Olive pomace had the highest reactivity value and the shortest total gasification time, as it contained the greatest amount of volatile matter (Table 1). Moreover, note how gasification reactivity at 50 and 90% of char conversion was higher when particle size decreased, which is in agreement with the reported literature.[22,33] The reactivity should decrease with increasing particle sizes as a consequence of an increase in the diffusion resistance in the gasification process. However, while R_{50} of olive stone was similar in the three sample sizes, the time required was higher when particle size increased. Thus, gasification could have been delayed due to heat and mass transfer problems caused by large particles. In general, an increase in the degree of conversion led to an increase in the reactivity caused by the mineral content in the raw materials. Alkali and alkaline earth metals captured within the carbon structure were continuously released during devolatilization, and, as this was continuous, the alkali metals became more concentrated in the solid phase, which led to a higher number of active sites of carbon. Thus, reactivity accelerated as the reaction proceeded.[34]

Also, Figure 1f displays char conversion obtained from gasification of both samples for different particle sizes. The biomass had a significant influence on the time required for reaching a plateau for all conversion curves. In fact, there was a constant conversion rate (50%) for olive pomace between 5 and 10 min depending on particle size, whereas, for olive stone, this was achieved after 30 min. The reactivity results can easily be linked to the volatile matter content in the raw material. As expected, among the range of particle sizes researched, the larger particles required more time for reaching constant conversion in both biomasses due to increased resistance to diffusion.[32]

Finally, the effect of the particle size in the olive waste on the main gases released during gasification was analyzed. Figure 2 plots the gas yields calculated by integrating the data measured using a mass spectrometer during gasification. H_2, CO, CO_2, CH_4, and C_2H_4 were assumed to be the main components of the fuel gas produced. The main reactions involved during gasification are summarized below.

Primary reactions

$$C + H_2O \rightleftarrows CO + H_2 \quad \text{char gasification}$$

$$C + 2H_2O \rightleftarrows CO_2 + 2H_2 \quad \text{char gasification}$$

Secondary reactions

$$CO + H_2O \rightleftarrows CO_2 + H_2 \quad \text{water} - \text{gas shift}$$

$$CH_4 + H_2O \rightleftarrows CO + 3H_2 \quad \text{steam reforming}$$

https://doi.org/10.1021/acs.iecr.1c00688
Ind. Eng. Chem. Res. 2021, 60, 7505−7515

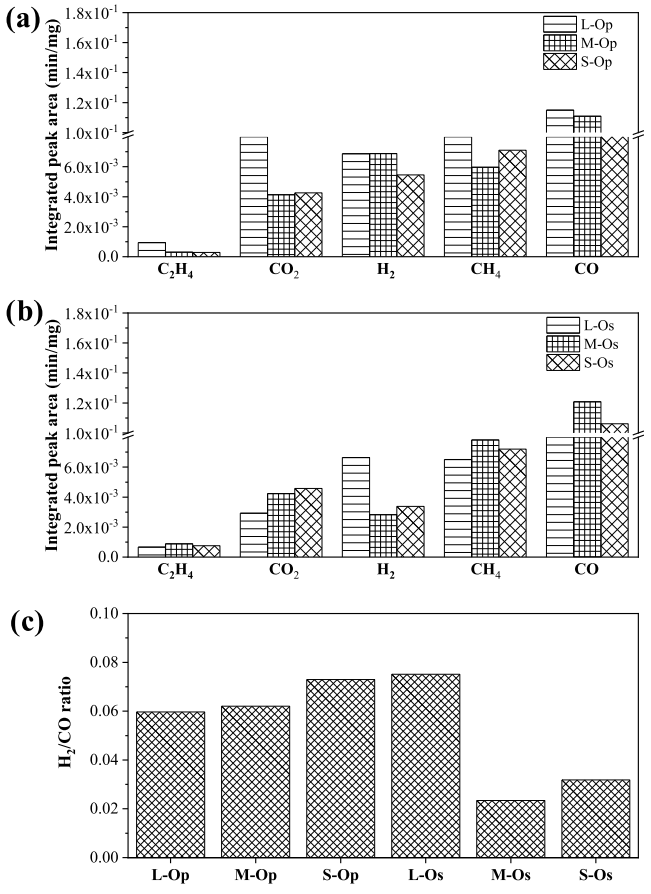

Figure 2. Main gaseous products formed during gasification as a function of particle size: (a) olive pomace, (b) olive stone, and the (c) H_2/CO ratio obtained in gasification.

$$C_nH_m \rightleftarrows C_{n-x}H_{m-y} + H_2 + CH_4 + C \quad \text{thermal cracking}$$

$$C + 2H_2 \rightleftarrows CH_4 \quad \text{methanation}$$

$$C + CO_2 \rightleftarrows 2CO \quad \text{Boudouard}$$

Regarding the olive pomace, in general, the gases tended to increase as particles became larger. Nevertheless, an inverse relationship, (except for CO_2) was found in other research in which an increase in these gases was reported when particle size decreased due to tar cracking and reforming reactions and the significant reduction in resistance to diffusion.[35−39] However, it should be noted that an increase in the particle size of olive pomace also meant it was more likely to contain olive stone, which could be attributed to the interaction between both raw materials. In addition, the olive stone was more uniform in form and size, which could have enhanced the gas−solid contact in the heterogeneous reaction.[40]

As for the olive stone, a rising trend was observed for H_2 and CO_2 when particle size increased from 0.85−1.4 to 1.4−2 mm, whereas CO decreased, which may be linked to equilibrium in the water−gas shift reaction and the Boudouard reaction.[40] Also, CH_4 content increased when particle size increased from 0.85−1.4 to 1.4−2 mm, which indicated that the kinetics of the methanation reaction slowed down with larger particle size.[45,46] Nevertheless, the same trend was not seen in the largest particle size. As the particle size of the olive stone increased, it became more homogeneous in shape and size, which might have enhanced the water−gas shift reaction and, thus, produced more H_2.[41] In addition, large particles tended to have a lower biomass consumption rate. This was an important point in this study due to the low weight and large size of the biomass studied.

Finally, Figure 2c displays the H_2/CO ratio calculated from the MS analysis of the effluent gases from gasification. This ratio was an important factor in gasification since it determined syngas quality and hence, in turn, how the effluent gas could be used. Opposite trends can be seen with the olive stone and olive pomace. With the latter, a slight downward trend can be seen with particle size. However, with the former, the highest value was obtained for large particle size.

In short, for the olive pomace biomass, the small particle size (S-Op) was selected as it had the best reactivity and the H_2/CO ratio, whereas for the olive stone biomass, the larger particle size was chosen. This was because, even though gasification was slightly slower, as was reactivity, there was a considerable difference in the H_2/CO ratio. It must also be stressed that large particles predominated in the olive stone particle size distribution (61, 33, and 6 wt % for L-Os, M-Os, and S-Os, respectively). Therefore, using large particles could be of greater interest when scaling-up gasification in industry. Once the samples were established, the effect of the diatomaceous earth on gasification was evaluated.

3.1.2. Effect of Diatomaceous Earth during Gasification of Olive Waste. Figure 3a shows the TGA profile corresponding to the diatomaceous earth. As can be seen, the diatomaceous earth only showed weight loss at the pyrolysis stage and was stable during gasification. Figure 3b

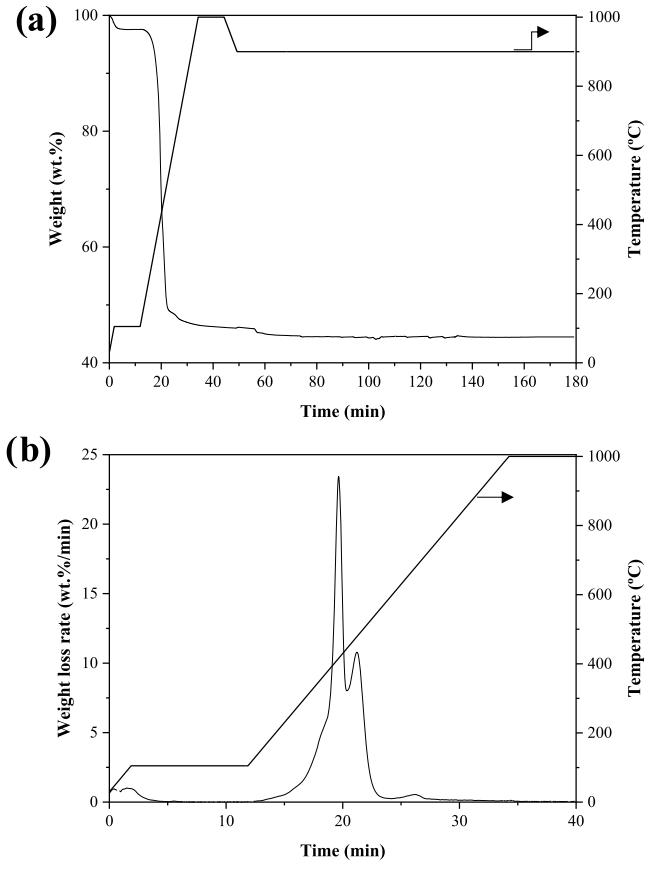

Figure 3. (a) TGA curves for diatomaceous earth gasification and (b) DTG curves for pyrolysis of diatomaceous earth.

https://doi.org/10.1021/acs.iecr.1c00688
Ind. Eng. Chem. Res. 2021, 60, 7505−7515

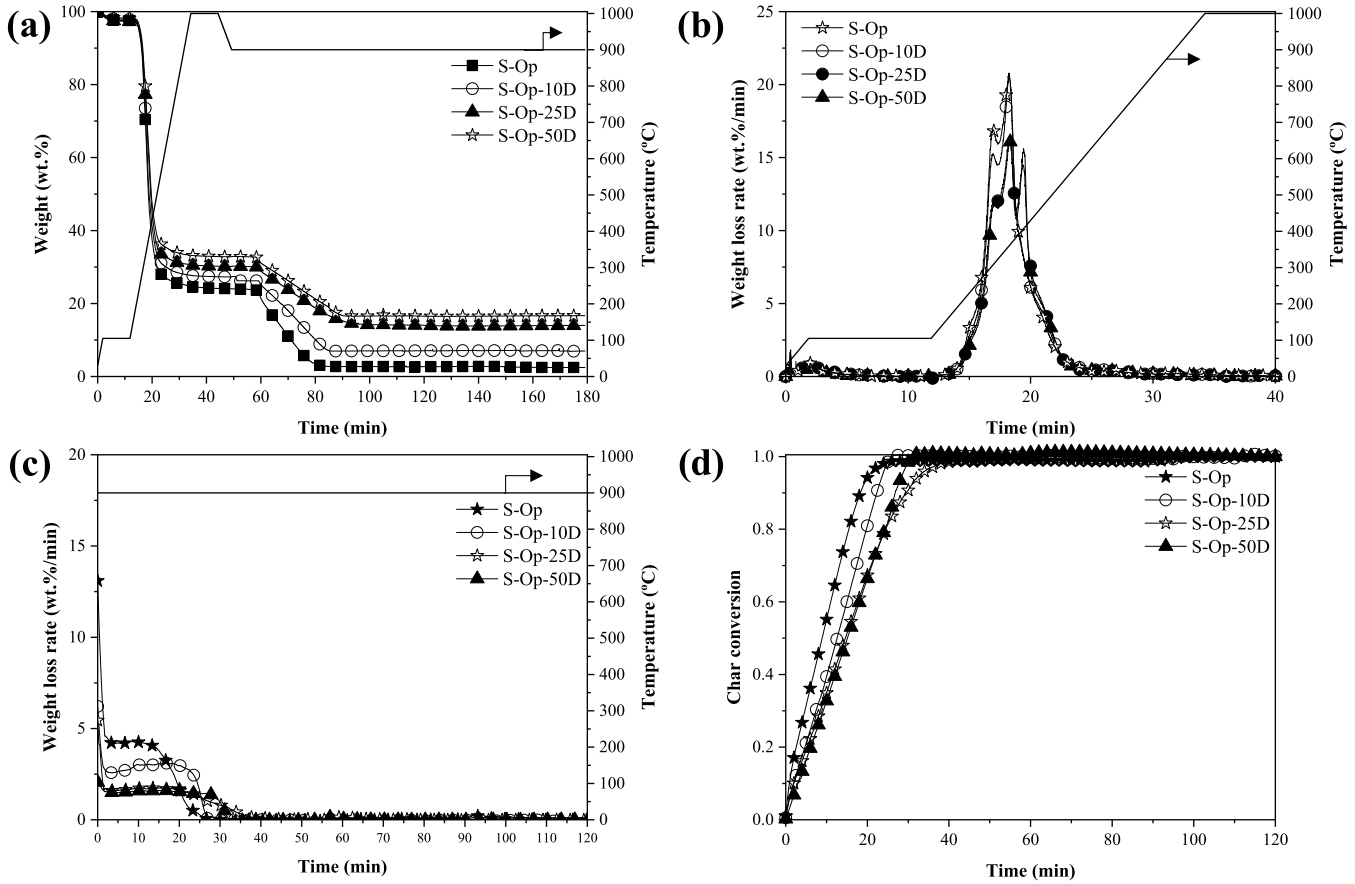

Figure 4. Gasification of olive pomace as a function of the percentage of diatomaceous earth: (a) TGA curves for gasification, (b) DTG curves for pyrolysis, (c) DTG curves for gasification, and (d) char conversion vs time plots for gasification.

shows the DTG curve for the pyrolysis stage at which four peaks were distinguished, which corresponded to different thermal decomposition stages. At the first peak (which was from room temperature to 105 °C), a very slight weight loss was observed due to the silica dehydrating.[42,43] The second peak (150−450 °C) was characterized by major weight loss, which might be a result of organic matter degradation.[43,44] The third peak (450−600 °C) could be associated with magnesium carbonate decomposition.[42,45] Finally, the fourth peak was observed at temperatures above 600 °C and may be related to endothermic reactions in the formation of magnesium and calcium silicate[46] and the decomposition calcium sulfate and carbonate.[42,43,47−49] The DTG curve at the gasification stage was not shown because, as mentioned above, the samples were stable at this point. Finally, the remaining residue from gasification was around 45 wt %, which indicated that about half had decomposed.

Figure 4 shows the TGA/DTG profiles for olive pomace gasification for the samples selected with and without diatomaceous earth. As expected, weight loss at the pyrolysis stage was higher than in gasification in all of the samples under study. Moreover, the amount of char obtained was higher in samples that contained more diatomaceous earth as it had not totally decomposed.

As for the pyrolysis stage (Figure 4b), note that at the main stage of pyrolysis, with olive pomace there were two main peaks. In this respect, the olive pomace sample containing 10 wt % diatomaceous earth (S-Op-10D) had a similar profile to the one in which the two peaks mentioned above were seen. However, as this percentage rose, three peaks were observed, the third of which corresponded to the third one that was a characteristic of the diatomaceous earth.

Regarding the gasification stage (Figure 4c), as the olive pomace sample contained diatomaceous earth, gasification was delayed at higher times. However, this behavior only became significant when the amount of diatomaceous earth increased from 0 to 25 wt %, above which slight differences were observed. Table 4 lists gasification reactivity at 50 and 90% of conversion (R_{50} and R_{90}, respectively) and the time required (t_{50} and t_{90}, respectively). As mentioned above, the higher the amount of earth, the higher the t_{50} and t_{90} and the lower the R_{50} and R_{90}. This may be associated with the effect of K and Si on gasification. The positive effect of K is well known, whose rapid diffusion through the carbon matrix can lead to the

Table 4. Gasification Reactivity for Olive Pomace and Olive Stone as a Function of the Percentage of Diatomaceous Earth

sample	R_{50} (1/min)	t_{50} (min)	R_{90} (1/min)	t_{90} (min)
S-Op	0.11	5.6	0.39	13.5
S-Op-10D	0.08	12.6	0.38	22.3
S-Op-25D	0.06	14.6	0.27	29.5
S-Op-50D	0.06	15.1	0.31	26.8
L-Os	0.03	41.4	0.16	70.1
L-Os-10D	0.02	43.6	0.27	69.1
L-Os-25D	0.03	48.4	0.27	64.1
L-Os-50D	0.02	62.3	0.37	91.3

https://doi.org/10.1021/acs.iecr.1c00688
Ind. Eng. Chem. Res. 2021, 60, 7505−7515

formation of micropores or mesopores, which increases the reaction rate and gasification reactivity.[50,51] Thus, an increase in K should enhance gasification reactivity. In this respect, Figure 5a shows the trend in reactivity as a function of K in the olive pomace samples. An increase in K clearly reduced gasification reactivity whose cause may have been twofold: olive pomace had the highest content of K (as shown in Table 1), and thus, adding diatomaceous earth only accounted for 3 wt % of the total (from 23.0 to 23.7 g/L for S-Op and S-Op-50D, respectively), which could be considered negligible; second, the high content of Si could have promoted deactivation of K as a catalyst.[52,53] In this study, olive pomace was high in Si (Table 1), which increased fivefold on adding diatomaceous earth. Thus, Si was more significant than K, which might explain why gasification reactivity did not improve when diatomaceous earth was added to the olive pomace. Moreover, as expected, gasification reactivity was enhanced as the process continued, which could be linked to the increase in metal content, as devolatilization occurred. In addition, although S-Op-10D had lower R_{50} than S-Op, they both had similar results for R_{90}. This might have been because the olive pomace continuously decomposed during gasification. Afterward, the diatomaceous earth became more concentrated in the sample, thereby enhancing contact between the olive pomace and the alkali and alkali earth metals, and, hence, gasification reactivity, in turn. Similar behavior was observed on comparing S-Op-25D and S-Op-50D, which had a similar R_{50}, but a rather different R_{90}. These reactivity results were corroborated with those for char conversion (Figure 4d), which was constant (50% of conversion) at around 5 min for S-Op; whereas in the samples with diatomaceous earth, this was only achieved after 13 min.

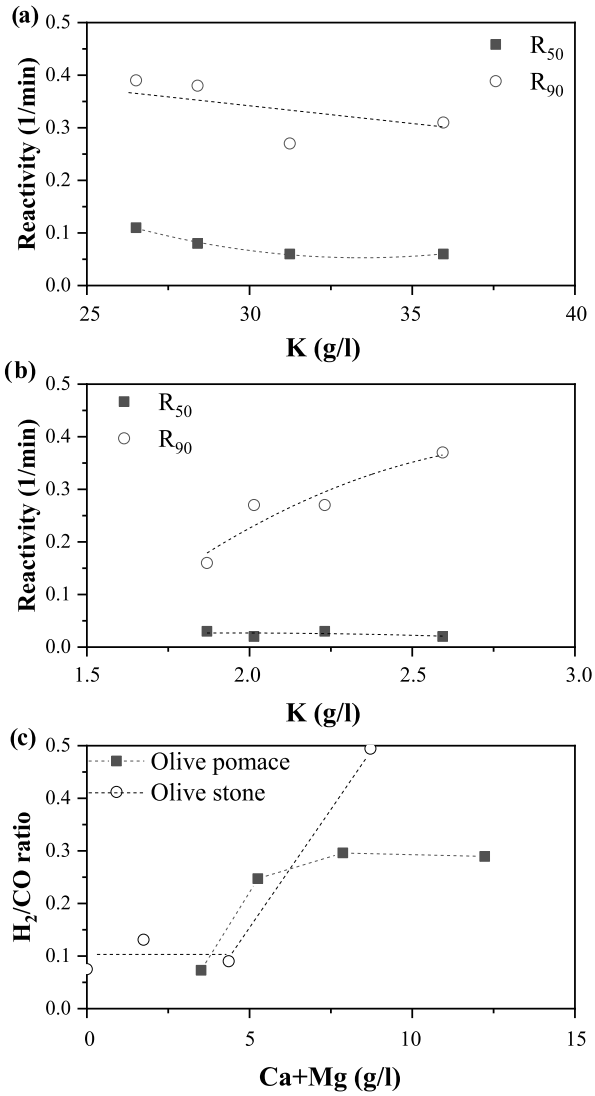

Figure 5. Evolution of gasification reactivity and H_2/CO as a function of alkali (K) and alkaline earth (Ca + Mg) metals: (a) olive pomace reactivity, (b) olive stone reactivity, and the (c) H_2/CO ratio.

Concerning olive stone, Figure 6 shows the TGA/DTG profiles for olive stone gasification with and without diatomaceous earth. Just like with olive pomace, weight loss at the pyrolysis stage was higher than during gasification in all of the samples, and the amount of char obtained was higher in those samples that contained a higher proportion of diatomaceous earth as it had not totally decomposed. In addition, weight loss at the gasification stage for L-Os-50D was clearly significantly lower and occurred more slowly than in the other samples containing diatomaceous earth. Figure 6b shows the DTG curve for the pyrolysis stage of olive stone gasification with and without diatomaceous earth. Olive stone containing diatomaceous earth displayed a similar profile to that for olive stone. However, as the amount of earth increased in the sample, the third peak which characterized its decomposition became more marked.

Now, focusing on the gasification stage (Figure 6c), diatomaceous earth in the olive stone sample delayed gasification at higher times, albeit not to the extent as seen in olive pomace. Also, Table 4 lists gasification reactivity at 50 and 90% of conversion (R_{50} and R_{90}, respectively) and the time required (t_{50} and t_{90}, respectively). Unlike with olive pomace, R_{50} remained practically constant with more diatomaceous earth, while t_{50} was higher than it was in olive stone. However, as the process continued, reactivity increased, and higher values for R_{90} were obtained. This behavior was similar to that seen with olive pomace. Figure 5b shows the trend in reactivity as a function of K in the olive stone samples. Here, adding K improved R_{90} significantly as it accounted for about 40 wt % of the total (from 1.87 to 2.59 g/L for L-Os and L-Os-50D, respectively). Moreover, although when diatomaceous earth was added, Si content also increased, and such high values as those seen in the olive pomace were not reached. Therefore, there was less possibility of deactivating K (Table 1). Even so, the positive effect of the diatomaceous earth was more pronounced in olive stone, as higher reactivity values were obtained, and thus less time was required. One interesting finding was that although L-Os-50D obtained the highest R_{90}, the time required for achieving this conversion was also the highest. This may be linked to the slow but constant weight loss, which can be observed in Figure 6d, which shows char conversion for olive stone. Note that at low degrees of conversion, the olive stone required lesser time than in the sample containing diatomaceous earth. However, as gasification progressed, the curves overlapped. In this respect, the samples L-Os and L-Os-10D overlapped at a 50% rate of conversion, while L-Os-25D converged with these two samples at 70% of conversion. Finally, L-Os-50D was the sample with the most stable increase in conversion.

In addition, the effect of diatomaceous earth on outlet-gas composition was studied. Figure 7 displays the integrated peak

https://doi.org/10.1021/acs.iecr.1c00688
Ind. Eng. Chem. Res. 2021, 60, 7505−7515

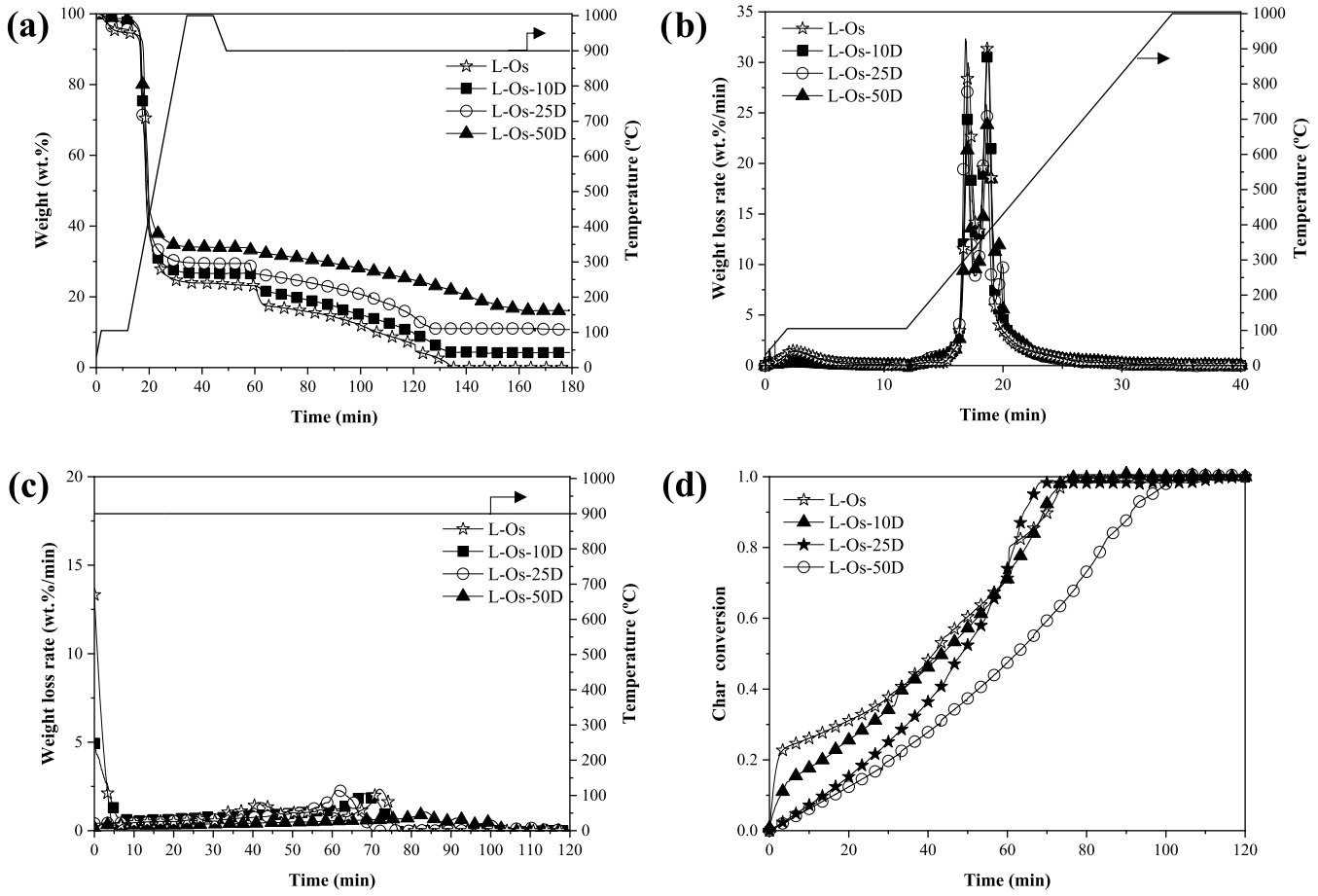

Figure 6. Gasification of olive stone as a function of the percentage of diatomaceous earth: (a) TGA curves for gasification, (b) DTG curves for pyrolysis, (c) DTG curves for gasification, and (d) char conversion vs time plots for gasification.

areas of the main gases given off during gasification. In general, diatomaceous earth clearly improved the H_2 yield. In addition, a decrease in the amount of CO and CH_4 given off was also detected. This could be explained by the promotion of the water−gas shift reaction that may have been catalyzed by Ca and Mg in the diatomaceous earth.[13,14,54,55] The decrease in CH_4 might have been caused by the diatomaceous earth inhibiting the methanation reaction and promoting steam reformation. Finally, CO_2 emissions showed opposite trends depending on the raw material. With olive stone, an increase in CO_2 emissions was observed when the amount of diatomaceous earth increased in the sample, which may have been linked to the enhanced water−gas shift and Boudouard reactions. However, with olive pomace, the opposite trend was seen, which indicated that the effect of diatomaceous earth was less predominant in olive pomace, which agreed well with the results obtained in the gasification reactivity process.

Finally, syngas quality was analyzed by calculating the H_2/CO ratio. Figure 7c shows the effect diatomaceous earth had on the H_2/CO ratio. Evidently, the diatomaceous earth enhanced syngas quality. This was mainly because of its Ca and Mg content, which promoted the water−gas shift reaction.[10,11,49,50] Figure 5c shows the trend in the H_2/CO ratio as a function of Ca + Mg content in both olive pomace and olive stone. Note that the higher the Ca + Mg content, the higher the H_2/CO ratio was in both raw materials. Nonetheless, behavior varied depending on the biomass used. In olive pomace, equilibrium was achieved at 7.50 g/L, and thus, any increase above this value did not enhance this ratio. This meant that the increase in diatomaceous earth from 10 to 50 wt % did not improve syngas quality. As for olive stone, two clear trends could be observed: a horizontal line was obtained for low alkaline earth metal content (<5 g/L); however above 5 g/L, the trend became notably positive. In short, the effect of diatomaceous earth was more evident with olive stone. This may have been due to two reasons. First, the larger particle size and slower decomposition of olive stone meant more time was required for total oxidation and, thus, the gases released had a higher contact period with the diatomaceous earth than those in olive pomace.[56] Second, the alkaline earth metals had a greater effect on the olive stone sample as it did not initially contain any metals (Table 1). Finally, it may be concluded that out of the olive pomace samples, S-Op-10D was the optimal blend since it showed similar reactivity but with a higher H_2/CO ratio than in S-Op. With the olive stone samples, L-Os-50D was the optimal one as higher reactivity and H_2/CO ratios were achieved than in L-Os.

4. CONCLUSIONS

The effect of diatomaceous earth on gasification of olive pomace and olive stone by means of TGA-MS was evaluated after which the following conclusions were drawn:

- Raw material and particle size had a great influence on gasification. The olive pomace sample showed higher reactivity than that for olive stone, which agreed well with the proximate analysis. As for the influence of

https://doi.org/10.1021/acs.iecr.1c00688
Ind. Eng. Chem. Res. 2021, 60, 7505−7515

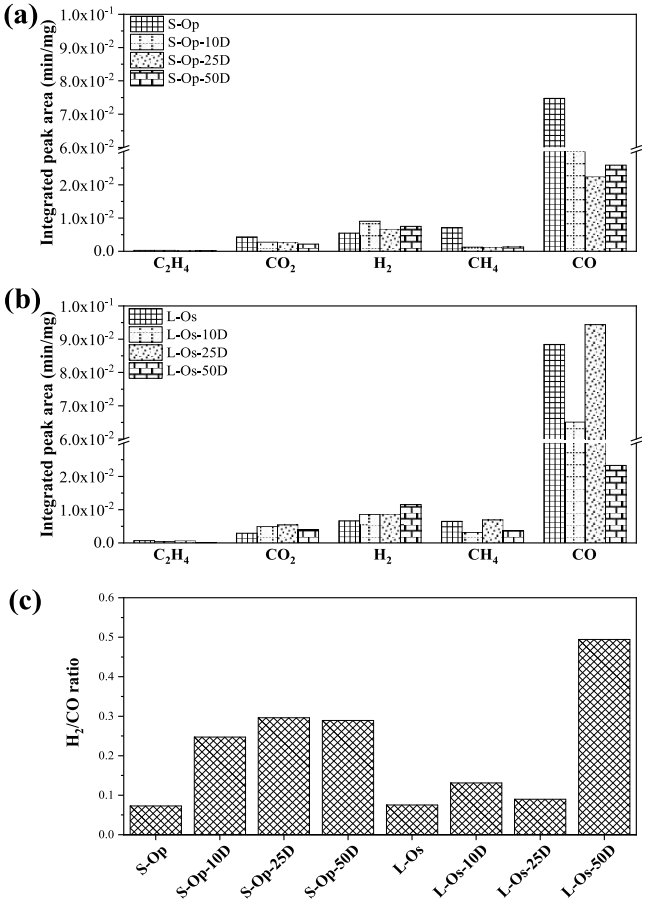

Figure 7. Main gaseous products formed during gasification as a function of the percentage of diatomaceous earth: (a) olive pomace, (b) olive stone, and the (c) H_2/CO ratio obtained in gasification.

particle size, in both biomasses, gasification was enhanced with smaller particles. Nonetheless, the H_2/CO ratio showed opposite trends depending on the feedstock used.

- Regarding gasification, diatomaceous earth delayed olive pomace and olive stone gasification at higher times. However, a distinct trend was observed in reactivity due to the different contributions made by alkali metals from the diatomaceous earth in the samples. In this respect, an increase in the diatomaceous earth was associated with an increase in K (mainly responsible for increasing reactivity) of 3 and 40 wt % in the olive pomace and olive stone samples, respectively. Therefore, due to the negligible contribution of K in the olive pomace samples, their reactivity did not improve, whereas in the olive stone, a significant increase in R_{90} was observed due to the higher contribution it made.
- Concerning the outlet-gas composition, diatomaceous earth improved the H_2 yield in both feedstocks. In addition, a decrease in the CO and CH_4 given off was also detected, while there was an inverse trend in CO_2 emissions.
- Also, the H_2/CO ratio was enhanced by diatomaceous earth since it increased the Ca + Mg content (mainly responsible for promoting the water−gas shift reaction) in the samples. Nevertheless, in the olive pomace, equilibrium was achieved 7.50 g/L, and thus, any value above this did not enhance the H_2/CO ratio, whereas in the olive stone, more than 5 g/L Ca + Mg was required to obtain a positive trend.
- Finally, the olive pomace sample with 10 wt % diatomaceous earth and the olive stone sample with 50 wt % showed optimum results as they had higher or similar reactivity, but they had a higher H_2/CO ratio than that found in their parents.

AUTHOR INFORMATION

Corresponding Author

Luz Sanchez-Silva − *Department of Chemical Engineering, University of Castilla−La Mancha, 13071 Ciudad Real, Spain;* orcid.org/0000-0002-4348-7520; Phone: +34 926 29 53 00; Email: marialuz.sanchez@uclm.es; Fax: +34 926 29 52 56

Authors

María Puig-Gamero − *Department of Chemical Engineering, University of Castilla−La Mancha, 13071 Ciudad Real, Spain*

Paula Sánchez − *Department of Chemical Engineering, University of Castilla−La Mancha, 13071 Ciudad Real, Spain*

Complete contact information is available at: https://pubs.acs.org/10.1021/acs.iecr.1c00688

Funding

Spanish government (Grant No. FPU15/02653), European Regional Development Fund (TEQUIMA group), and the Regional Government of Castilla-La Mancha (Project SPBLY/17/180501/000238)

Notes

The authors declare no competing financial interest.

ACKNOWLEDGMENTS

The authors would like to thank the Spanish government for their financial support (Grant No. FPU15/02653) and the Aceites Garcia de la Cruz olive oil mill.

ABBREVIATIONS

Op	olive pomace
Os	olive stone
d	diatomaceous earth
TGA	thermogravimetric analysis
DTG	derivative thermogravimetric
MS	mass spectrometry
ICP	inductively coupled plasma spectrometry
R_{50}	reactivity at 50 % of char conversion
R_{90}	reactivity at 90% of char conversion

REFERENCES

(1) Commission, E. *Short-Term Outlook for EU Agricultural Markets* (accessed 17 March, 2020).

(2) Cequier, E.; Aguilera, J.; Balcells, M.; Canela-Garayoa, R. Extraction and characterization of lignin from olive pomace: a comparison study among ionic liquid, sulfuric acid, and alkaline treatments. *Biomass Convers. Biorefin.* **2019**, *9*, 241−252.

(3) Bas, F. J.; Colinet-Carmona, M.; LoboGarcia, J. In *The Olive Tree as an Energy Source in the Mediterranean Area: Andalusia*, Proceedings of the First World Conference on Biomass for Energy and Industry, Seville, 2000; pp 5−9.

(4) Azbar, N.; Bayram, A.; Filibeli, A.; Muezzinoglu, A.; Sengul, F.; Ozer, A. A review of waste management options in olive oil production. *Crit. Rev. Environ. Sci. Technol.* **2004**, *34*, 209−247.
(5) Caputo, A. C.; Scacchia, F.; Pelagagge, P. M. Disposal of by-products in olive oil industry: waste-to-energy solutions. *Appl. Therm. Eng.* **2003**, *23*, 197−214.
(6) Sikarwar, V. S.; Zhao, M.; Fennell, P. S.; Shah, N.; Anthony, E. J. Progress in biofuel production from gasification. *Prog. Energy Combust. Sci.* **2017**, *61*, 189−248.
(7) Dogru, M.; Erdem, A. Autothermal Fixed Bed Updraft Gasification of Olive Pomace Biomass and Renewable Energy Generation via Organic Rankine Cycle Turbine: Green energy generation from waste biomass in the Mediterranean region. *Johnson Matthey Technol. Rev.* **2020**, *64*, 119−134.
(8) Ducom, G.; Gautier, M.; Pietraccini, M.; Tagutchou, J.-P.; Lebouil, D.; Gourdon, R. Comparative analyses of three olive mill solid residues from different countries and processes for energy recovery by gasification. *Renewable Energy* **2020**, *145*, 180−189.
(9) Rehman Zia, U. U.; Rashid, Tu.; Awan, W. N.; Hussain, A.; Ali, M. Quantification and technological assessment of bioenergy generation through agricultural residues in Punjab (Pakistan). *Biomass Bioenergy* **2020**, *139*, No. 105612.
(10) Kumabe, K.; Hanaoka, T.; Fujimoto, S.; Minowa, T.; Sakanishi, K. Co-gasification of woody biomass and coal with air and steam. *Fuel* **2007**, *86*, 684−689.
(11) González-Vázquez, M. P.; García, R.; Gil, M. V.; Pevida, C.; Rubiera, F. Comparison of the gasification performance of multiple biomass types in a bubbling fluidized bed. *Energy Convers. Manage.* **2018**, *176*, 309−323.
(12) Castro, C.; Mota, A.; Ribeiro, A.; Soares, M.; Araujo, J.; Carvalho, J.; Vilarinho, C. *Potential of Exhausted Olive Pomace for Gasification*; CRC Press, 2018.
(13) Puig-Gamero, M.; Lara-Díaz, J.; Valverde, J. L.; Sánchez, P.; Sanchez-Silva, L. Synergestic effect in the steam co-gasification of olive pomace, coal and petcoke: Thermogravimetric-mass spectrometric analysis. *Energy Convers. Manage.* **2018**, *159*, 140−150.
(14) Puig-Gamero, M.; Lara-Díaz, J.; Valverde, J. L.; Sanchez-Silva, L.; Sánchez, P. Dolomite effect on steam co-gasification of olive pomace, coal and petcoke: TGA-MS analysis, reactivity and synergistic effect. *Fuel* **2018**, *234*, 142−150.
(15) Almeida, A.; Neto, P.; Pereira, I.; Ribeiro, A.; Pilão, R. Effect of temperature on the gasification of olive bagasse particles. *J. Energy Inst.* **2019**, *92*, 153−160.
(16) Cardoso, J.; Silva, V.; Eusebio, D.; Trninić, M. R.; Carvalho, T.; Brito, P. Techno-economic analysis of olive pomace gasification for cogeneration applications in small facilities. *Therm. Sci.* **2019**, *23*, 1487−1498.
(17) Zhang, Z.; Pang, S.; Levi, T. Influence of AAEM species in coal and biomass on steam co-gasification of chars of blended coal and biomass. *Renewable Energy* **2017**, *101*, 356−363.
(18) Sanchez-Silva, L.; López-González, D.; Garcia-Minguillan, A. M.; Valverde, J. L. Pyrolysis, combustion and gasification characteristics of Nannochloropsis gaditana microalgae. *Bioresour. Technol.* **2013**, *130*, 321−331.
(19) Jones, J. M.; Harding, A. W.; Brown, S. D.; Thomas, K. M. Detection of reactive intermediate nitrogen and sulfur species in the combustion of carbons that are models for coal chars. *Carbon* **1995**, *33*, 833−843.
(20) López-González, D.; Fernandez-Lopez, M.; Valverde, J. L.; Sanchez-Silva, L. Gasification of lignocellulosic biomass char obtained from pyrolysis: Kinetic and evolved gas analyses. *Energy* **2014**, *71*, 456−467.
(21) Mandapati, R. N.; Daggupati, S.; Mahajani, S. M.; Aghalayam, P.; Sapru, R. K.; Sharma, R. K.; Ganesh, A. Experiments and kinetic modeling for CO2 gasification of indian coal chars in the context of underground coal gasification. *Ind. Eng. Chem. Res.* **2012**, *51*, 15041−15052.
(22) Gómez-Barea, A.; Ollero, P.; Fernández-Baco, C. Diffusional effects in CO2 gasification experiments with single biomass char particles. 1. Experimental investigation. *Energy Fuels* **2006**, *20*, 2202−2210.
(23) Mitsuoka, K.; Hayashi, S.; Amano, H.; Kayahara, K.; Sasaoaka, E.; Uddin, M. A. Gasification of woody biomass char with CO2: The catalytic effects of K and Ca species on char gasification reactivity. *Fuel Process. Technol.* **2011**, *92*, 26−31.
(24) Zhang, Y.; Hara, S.; Kajitani, S.; Ashizawa, M. Modeling of catalytic gasification kinetics of coal char and carbon. *Fuel* **2010**, *89*, 152−157.
(25) Cabeza, A.; Sobrón, F.; Yedro, F.; García-Serna, J. Autocatalytic kinetic model for thermogravimetric analysis and composition estimation of biomass and polymeric fractions. *Fuel* **2015**, *148*, 212−225.
(26) Sanchez-Silva, L.; López-González, D.; Villaseñor, J.; Sánchez, P.; Valverde, J. L. Thermogravimetric-mass spectrometric analysis of lignocellulosic and marine biomass pyrolysis. *Bioresour. Technol.* **2012**, *109*, 163−172.
(27) Zhou, C.; Liu, G.; Wang, X.; Qi, C. Co-combustion of bituminous coal and biomass fuel blends: Thermochemical characterization, potential utilization and environmental advantage. *Bioresour. Technol.* **2016**, *218*, 418−427.
(28) Edreis, E. M.; Luo, G.; Li, A.; Xu, C.; Yao, H. Synergistic effects and kinetics thermal behaviour of petroleum coke/biomass blends during H 2 O co-gasification. *Energy Convers. Manage.* **2014**, *79*, 355−366.
(29) Puig-Gamero, M.; Alcazar-Ruiz, Á.; Sánchez, P.; Sanchez-Silva, L. Binary Blends Versus Ternary Blends in Steam Cogasification by Means of TGA−MS: Reactivity and H2/CO Ratio. *Ind. Eng. Chem. Res.* **2020**, *59*, 12801−12811.
(30) Ong, H. C.; Chen, W.-H.; Singh, Y.; Gan, Y. Y.; Chen, C.-Y.; Show, P. L. A state-of-the-art review on thermochemical conversion of biomass for biofuel production: A TG-FTIR approach. *Energy Convers. Manage.* **2020**, *209*, No. 112634.
(31) Niu, S.; Zhou, Y.; Yu, H.; Lu, C.; Han, K. Investigation on thermal degradation properties of oleic acid and its methyl and ethyl esters through TG-FTIR. *Energy Convers. Manage.* **2017**, *149*, 495−504.
(32) Tripathi, M.; Sahu, J. N.; Ganesan, P. Effect of process parameters on production of biochar from biomass waste through pyrolysis: A review. *Renewable Sustainable Energy Rev.* **2016**, *55*, 467−481.
(33) Mani, T.; Murugan, P.; Abedi, J.; Mahinpey, N. Pyrolysis of wheat straw in a thermogravimetric analyzer: effect of particle size and heating rate on devolatilization and estimation of global kinetics. *Chem. Eng. Res. Des.* **2010**, *88*, 952−958.
(34) Chen, J.; Fan, Y.; E, J.; Cao, W.; Zhang, F.; Gong, J.; Liu, G.; Xu, W. Effects analysis on the gasification kinetic characteristics of food waste in supercritical water. *Fuel* **2019**, *241*, 94−104.
(35) Mallick, D.; Mahanta, P.; Moholkar, V. S. Co−gasification of coal/biomass blends in 50 kWe circulating fluidized bed gasifier. *J. Energy Inst.* **2020**, *93*, 99−111.
(36) Hernández, J. J.; Aranda-Almansa, G.; Bula, A. Gasification of biomass wastes in an entrained flow gasifier: Effect of the particle size and the residence time. *Fuel Process. Technol.* **2010**, *91*, 681−692.
(37) Janajreh, I.; Al Shrah, M. Numerical and experimental investigation of downdraft gasification of wood chips. *Energy Convers. Manage.* **2013**, *65*, 783−792.
(38) Chen, G.; Andries, J.; Luo, Z.; Spliethoff, H. Biomass pyrolysis/gasification for product gas production: the overall investigation of parametric effects. *Energy Convers. Manage.* **2003**, *44*, 1875−1884.
(39) Fremaux, S.; Beheshti, S.-M.; Ghassemi, H.; Shahsavan-Markadeh, R. An experimental study on hydrogen-rich gas production via steam gasification of biomass in a research-scale fluidized bed. *Energy Convers. Manage.* **2015**, *91*, 427−432.
(40) Beheshti, S. M.; Ghassemi, H.; Shahsavan-Markadeh, R. Process simulation of biomass gasification in a bubbling fluidized bed reactor. *Energy Convers. Manage.* **2015**, *94*, 345−352.

https://doi.org/10.1021/acs.iecr.1c00688
Ind. Eng. Chem. Res. 2021, 60, 7505−7515

(41) Lim, M. T.; Alimuddin, Z. Bubbling fluidized bed biomass gasification—Performance, process findings and energy analysis. *Renewable Energy* **2008**, *33*, 2339−2343.
(42) Verdeja González, L. F.; Sancho Martínez, J. P.; Queneche, B.; Luis, J.; Vásquez Arrieta, E. R. Características fisicoquímicas de las diatomitas de Bayovar (Peru). *Bol. Soc. Esp. Ceram. Vidrio* **1990**, *29*, 87−93.
(43) Zheng, R.; Ren, Z.; Gao, H.; Zhang, A.; Bian, Z. Effects of calcination on silica phase transition in diatomite. *J. Alloys Compd.* **2018**, *757*, 364−371.
(44) Dai, S.; Zhang, L.; Hao, C.; Qi, P.; Wang, G.; Ma, W. Preparation and characterization of zeolite/diatomite composite materials. *Mater. Res. Express* **2019**, *6*, No. 125516.
(45) Devasahayam, S.; Strezov, V. Thermal decomposition of magnesium carbonate with biomass and plastic wastes for simultaneous production of hydrogen and carbon avoidance. *J. Cleaner Prod.* **2018**, *174*, 1089−1095.
(46) Risnes, H.; Fjellerup, J.; Henriksen, U.; Moilanen, A.; Norby, P.; Papadakis, K.; Posselt, D.; Sørensen, L. H. Calcium addition in straw gasification☆. *Fuel* **2003**, *82*, 641−651.
(47) Kuusik, R.; Salkkonen, P.; Niinistö, L. Thermal decomposition of calcium sulphate in carbon monoxide. *J. Therm. Anal.* **1985**, *30*, 187−193.
(48) Han, L.; Wang, Q.; Ma, Q.; Yu, C.; Luo, Z.; Cen, K. Influence of CaO additives on wheat-straw pyrolysis as determined by TG-FTIR analysis. *J. Anal. Appl. Pyrolysis* **2010**, *88*, 199−206.
(49) Wang, D.; Xiao, R.; Zhang, H.; He, G. Comparison of catalytic pyrolysis of biomass with MCM-41 and CaO catalysts by using TGA−FTIR analysis. *J. Anal. Appl. Pyrolysis* **2010**, *89*, 171−177.
(50) Virla, L. D.; Montes, V.; Wu, J.; Ketep, S. F.; Hill, J. M. Synthesis of porous carbon from petroleum coke using steam, potassium and sodium: Combining treatments to create mesoporosity. *Microporous Mesoporous Mater.* **2016**, *234*, 239−247.
(51) Arnold, R.; Hill, J. Catalysts for gasification: a review. *Sustainable Energy Fuels* **2019**, *3*, 656−672.
(52) Fan, Y.; Zhang, H.; Lyu, Q.; Zhu, Z. Investigation of slagging characteristics and anti-slagging applications for Indonesian coal gasification. *Fuel* **2020**, *267*, No. 117285.
(53) Cabuk, B.; Duman, G.; Yanik, J.; Olgun, H. Effect of fuel blend composition on hydrogen yield in co-gasification of coal and non-woody biomass. *Int. J. Hydrogen Energy* **2020**, *45*, 3435−3443.
(54) Widyawati, M.; Church, T. L.; Florin, N. H.; Harris, A. T. Hydrogen synthesis from biomass pyrolysis with in situ carbon dioxide capture using calcium oxide. *Int. J. Hydrogen Energy* **2011**, *36*, 4800−4813.
(55) Hervy, M.; Olcese, R.; Bettahar, M. M.; Mallet, M.; Renard, A.; Maldonado, L.; Remy, D.; Mauviel, G.; Dufour, A. Evolution of dolomite composition and reactivity during biomass gasification. *Appl. Catal., A* **2019**, *572*, 97−106.
(56) Yin, R.; Liu, R.; Wu, J.; Wu, X.; Sun, C.; Wu, C. Influence of particle size on performance of a pilot-scale fixed-bed gasification system. *Bioresour. Technol.* **2012**, *119*, 15−21.

https://doi.org/10.1021/acs.iecr.1c00688
Ind. Eng. Chem. Res. 2021, 60, 7505−7515